THE EXTENDED FINITE ELEMENT METHOD APPLIED TO CRACK GROWTH MECHANISM OF ASPHALT PAVEMENT

Seongmun Yu, Chau Dinh Thanh, Sungho Mun,
Hyunjong Lee, Seungjung Lee, Goangseup Zi*
Department of civil, environmental and architectural engineering
Korea University
5 Ga 1 An-Am Dong, Seoul, Korea
g-zi@korea.ac.kr

ABSTRACT

This paper studies static and fatigue crack growth of asphalt using the extended finite element method(XFEM). XFEM is a useful method to analyze the crack growth and stress distribution without remeshing. Static crack growth and stress distribution have been studied along with XFEM and cohesive crack model. In accordance with these results, load-displacement curve and fracture energy of specimen are obtained in three different temperatures. In this paper, Paris' law is used to analyze fatigue crack growth. The analysis gives N-a curve for simulation of crack growth, and the curve almost corresponds with test results. In order to take appropriate load velocity and temperature effect into consideration, viscoelasticity characteristics of asphalt may be studied in additional study hereafter.

1. INTRODUCTION

Asphalt pavements can be cracked under repeated vehicle loadings even if the load is far below the strength limit, which is called fatigue crack of asphalt pavement. The fatigue cracks initiate from the pavement surface and propagate downward. As the crack reaches to the substrate, the pavements are deemed to be destroyed and need some repair or to be replaced. Therefore, precise prediction on the crack growth in the asphalt pavement is necessary for efficient maintenance works.

Computational modeling of crack growth has been studied by various techniques. Among the techniques, remeshing at the crack growth would be the simpliest choice. In this case, whenever the mesh is updated or remeshed, internal variables of the system need to be projected between different meshes, which may lead to inaccurate result of analysis. The intra-element method in which the direction of the crack is aligned with the edges of the elements can be considered (Xu et al. 1994; Ortiz et al. 1999) but it is also pointed out that the path or crack growth is influenced by the mesh.

Recently, such awkward problems encountered by remeshing methods are eliminated by meshless methods or extended finite element methods (XFEM). The XFEM, developed by Belytschko (Belytschko and Black. 1999), allows the crack to grow almost independently to the mesh. In other words, there is no need to change the mesh at every single step of crack growth. Because XFEM is an extended version of the conventional FEM, the method can fit in existing finite element codes with minimum modification. The method has been successfully used not only for static problems (Moes *et*

al., 1999, 2002; Zi *et al*., 2003; Zi *et al*., 2004), but also for dynamic problems (Belytschko *et al*., 2003; Zi *et al*., 2005).

In this paper, the static crack growth is analyzed by using the extended finite element method combined with the cohesive crack model. Regarding the fatigue crack growth and its simulation, the extended finite element method is combined with the Paris' law. The displacement fields extended to discontinuity in section 2 and the descretized equilibrium equations are derived in section 3. To demonstrate performance of the method, numerical simulation of experimental results is shown in the case of static and fatigue crack propagation in section 4 and 5, respectively. Conclusions are drawn in the last section.

2. ENRICHMENT FUNCTION AND DISPLACEMENT FIELD

2.1 Enrichment function

To describe a crack, additional parameters and functions are to be added to the displacement field of the conventional finite element approximation. Thus the displacement field is the combination of the conventional continuous one and the discontinuous one provided by the enrichment functions.

Two different kinds of enrichment functions are used to model the discontinuities. For an element completely cut by a crack, the enrichment function is a step function *H* which is defined as

$$H\left[f_I(\mathrm{X})\right]=\begin{cases}1 & for \quad f_I(\mathrm{X})>0\\ -1 & for \quad f_I(\mathrm{X})<0\end{cases} \tag{1}$$

Where $f_I(\mathrm{X})$ is a signed distance function defined as follow

$$f_I(\mathrm{X})=\begin{cases}sign\left[\mathrm{n}\cdot(\mathrm{X}_I-\mathrm{X})\min\left\|\mathrm{X}_I-\mathrm{X}\right\|\right] & for \quad \mathrm{X}_I\in W_b\\ \mathrm{n}\cdot\left(\mathrm{X}_{tip}-\mathrm{X}_I\right) & for \quad \mathrm{X}_I\in W_s\end{cases} \tag{2}$$

with W_b is a set of nodes of elements completely cut by the crack, and W_s is a set of nodes of elements containing the crack tip.

For an element partially cut by a crack, the enrichment functions are a set of branch functions *B*. In LEFM, these functions may be the asymptotic solutions of the displacement field near the crack tip

$$B=\sqrt{r}\left(\sin\frac{\theta}{2},\cos\frac{\theta}{2},\sin\frac{\theta}{2}\sin\theta,\cos\frac{\theta}{2}\sin\theta\right) \tag{3}$$

Where (*r*, θ) are the local polar coordinates at the tip.

In the case of the cohesive crack model, for which the crack tip singularity is not considered at the tip, the branch functions *B* is simplified to

$$B=r^m\sin\frac{\theta}{2},\quad \text{with } m=1,2,3,\ldots \tag{4}$$

2.2 Displacement field

In the XFEM, displacement fields u are sum of the continuous and the discontinuous displacement fields as follows

$$\mathrm{u} = \mathrm{u}_{cont} + \mathrm{u}_{disc} \tag{5}$$

with u_{cont} and u_{disc} are denoted to the continuous and the discontinuous part of the displacement field, respectively. Here, the continuous displacement field is approximated by the conventional FEM:

$$\mathrm{u}_{cont} = \sum_{I \in W(\mathrm{X})} N_I(\mathrm{X})\mathrm{u}_I \tag{6}$$

Where $W(\boldsymbol{X})$ are all the nodes, $N_I(\boldsymbol{X})$ is the shape functions and u_I is the nodal displacements. And the discontinuous part is given by

$$\mathrm{u}_{disc} = \sum_{I \in W_b(\mathrm{X})} N_I(\mathrm{X}) H(f_I(\mathrm{X}))a_I + \sum_{I \in W_S(\mathrm{X})} N_I(\mathrm{X}) \left(\sum_K B_K(\mathrm{X}) b_{IK} \right) \tag{7}$$

Where $H(f_I(\boldsymbol{X}))$ is the step function, $B(\boldsymbol{X})$ is the branch function, a_I and b_{IK} are additional parameters. So, the test functions and trial functions are defined as

$$\delta\mathrm{u} = \sum_{I \in W(\mathrm{X})} N_I(\mathrm{X}) \cdot \delta\mathrm{u}_I + \sum_{I \in W_b(\mathrm{X})} N_I(\mathrm{X}) \cdot H\left[f_I(\mathrm{X})\right] \cdot \delta a_I + \sum_{I \in W_s(\mathrm{X})} N_I(\mathrm{X}) \sum_K \left(B_K(\mathrm{X}) \cdot \delta\mathrm{b}_{IK}\right) \tag{8}$$

$$\mathrm{u} = \sum_{I \in W(\mathrm{X})} N_I(\mathrm{X}) \cdot \mathrm{u}_I + \sum_{I \in W_b(\mathrm{X})} N_I(\mathrm{X}) \cdot H\left[f_I(\mathrm{X})\right] \cdot a_I + \sum_{I \in W_s(\mathrm{X})} N_I(\mathrm{X}) \left(\sum_K B_K(\mathrm{X}) \cdot \mathrm{b}_{IK} \right) \tag{9}$$

In Equations (8) and (9), the first term is the approximation of the conventional FEM, while the second and the third terms represent discontinuities.

To decrease the area of the enriched domain and their number of additional parameters, the enriched function (1) and (4) can be modified by Equations (10) and (11) (Zi *et al*., 2003).

$$H_I(\boldsymbol{X}) = H(\boldsymbol{X}) - H(\boldsymbol{X}_I) \tag{10}$$

$$B_{IK}(\boldsymbol{X}) = B_K(\boldsymbol{X}) - B_K(\boldsymbol{X}_I) \tag{11}$$

Shifting of enrichment functions help enrichment displacements in elements not cut to be eliminated. But, notice that the shifting operation is effective for only the sign function $H_I(\boldsymbol{X})$ but not for the branch functions $B_{IK}(\boldsymbol{X})$.

3. GOVERNING EQUATION AND DISCRETIZED EQUATIONS

3.1 The governing equation of a continuum

From the equilibrium condition of a material point, the strong form of a continuum domain Ω_0 is as follows

$$\nabla \cdot \mathrm{P} + \rho_0 \mathrm{b} = 0 \quad \text{on} \quad \Omega_0 \notin \Gamma_0^c \tag{12}$$

where P is the stress tensor, $\rho_0\mathrm{b}$ is the body force. This Equation (12) is valid in the continuous

part of Ω_0 except the crack face Γ_0^c.

Boundary conditions are given by

$$\mathrm{u}(\mathrm{X}) = \bar{\mathrm{u}}(\mathrm{X}) \quad \text{on} \quad \Gamma_0^u \tag{13}$$

$$\mathrm{t}(\mathrm{X}) = \mathrm{n}_0 \cdot \mathrm{P}(\mathrm{X}) = \bar{\mathrm{t}}(\mathrm{X}) \quad \text{on} \quad \Gamma_0^t \tag{14}$$

$$\mathrm{n}_0 \cdot \mathrm{P}^- = -\mathrm{n}_0 \cdot \mathrm{P}^+ = \mathrm{t}_{c0} \quad \text{on} \quad \Gamma_0^c \tag{15}$$

Equation (13) is the Dirichlet boundary conditions (or the displacement boundary conditions) and Equation (14) is the Neumann boundary conditions (or external traction boundary conditions). Equation (15) is the traction condition on the crack face of the cohesive crack model.

We need to give a constitutive law relating the cohesive tractions to the crack opening displacement in the cohesive model as following

$$\mathrm{t}_{c0} = \mathrm{t}_{c0}(\llbracket \mathrm{u} \rrbracket) \quad \text{on} \quad \Gamma_0^c \tag{16}$$

Where $\llbracket \mathrm{u} \rrbracket$ is the crack opening displacement.

With n_0 is the unit normal towards outside of crack face. Note that

$$\Gamma_0^u \cup \Gamma_0^t \cup \Gamma_0^c = \Gamma_0 \tag{17}$$

$$\left(\Gamma_0^u \cap \Gamma_0^t\right) \cup \left(\Gamma_0^t \cap \Gamma_0^c\right) \cup \left(\Gamma_0^c \cap \Gamma_0^u\right) = \varnothing \tag{18}$$

3.2 Discretized governing equation

The weak form of equilibrium equations is given by

$$\delta W_{\mathrm{int}} = \delta W_{ext} \tag{19}$$

Where

$$\delta W_{\mathrm{int}} = \int_{\Omega_0 \notin \Gamma_0^c} (\nabla \cdot \delta \mathrm{u})^T : \mathrm{P} d\Omega \tag{20}$$

$$\delta W_{ext} = \int_{\Omega_0 \notin \Gamma_0^c} \rho_0 \cdot \delta \mathrm{u} \cdot \mathrm{b} \cdot d\Omega + \int_{\Gamma_0^t} \delta \mathrm{u} \cdot \bar{\mathrm{t}} d\Gamma + \int_{\Gamma_0^c} \llbracket \delta \mathrm{u} \rrbracket \cdot \mathrm{t}_{c0} d\Gamma \tag{21}$$

Here W_{int} is the internal work and W_{ext} is the external work. In Equation (21), the external work is caused by the body force, the applied tractions and the cohesive tractions respectively.

Substituting the test function and the trial function in Equations (8) and (9) into the weak form (19), one can obtain the discrete equilibrium equations

$$\mathrm{F}_I^{ext} = \mathrm{F}_I^{\mathrm{int}} \tag{22}$$

with

$$\mathrm{F}_I^{ext} = \begin{bmatrix} F_I^{u,ext} \\ F_I^{a,est} \\ F_{IK}^{b,ext} \end{bmatrix} = \begin{bmatrix} \int_{\Omega_0 \notin \Gamma_0^c} \rho_0 \cdot \mathrm{b} \cdot \mathrm{N}_I(\mathrm{X}) d\Omega + \int_{\Gamma_0^t} \bar{\mathrm{t}} \cdot \mathrm{N}_I(\mathrm{X}) d\Gamma + f_I^{u,cr} \\ \int_{\Omega_0 \notin \Gamma_0^c} \rho_0 \cdot \mathrm{b} \cdot \mathrm{N}_I(\mathrm{X}) \cdot H\left[f_I^{(n)}(\mathrm{X})\right] d\Omega + \int_{\Gamma_0^t} \bar{\mathrm{t}} \cdot \mathrm{N}_I(\mathrm{X}) H\left[f_I^{(n)}(\mathrm{X})\right] d\Gamma + f_I^{a,cr} \\ \int_{\Omega_0 \notin \Gamma_0^C} \rho_0 \cdot \mathrm{b} \cdot \mathrm{N}_I(\mathrm{X}) B_K^{(m)} d\Omega + \int_{\Gamma_0^t} \bar{\mathrm{t}} \cdot \mathrm{N}_I(\mathrm{X}) B_K^{(m)} d\Gamma + f_I^{b,cr} \end{bmatrix} \tag{23}$$

$$\mathrm{F}_I^{\mathrm{int}} = \begin{bmatrix} F_I^{u,\mathrm{int}} \\ F_I^{a,\mathrm{int}} \\ F_{IK}^{b,\mathrm{int}} \end{bmatrix} = \begin{bmatrix} \int_{\Omega_0 \notin \Gamma_0^c} \nabla \mathrm{N}_I(\mathrm{X}) \cdot P d\Omega \\ \int_{\Omega_0 \notin \Gamma_0^c} \left[\nabla \mathrm{N}_I(\mathrm{X}) \cdot H\left[f_I^{(n)}(\mathrm{X})\right] + \mathrm{N}_I(\mathrm{X}) \cdot \nabla H\left[f_I^{(n)}(X)\right]\right] \cdot P d\Omega \\ \int_{\Omega_0 \notin \Gamma_0^c} \left[\nabla \mathrm{N}_I(\mathrm{X}) \cdot B_K^{(m)} + \mathrm{N}_I(\mathrm{X}) \nabla B_K^{(m)}\right] \cdot P d\Omega \end{bmatrix} \tag{24}$$

4. STATIC CRACK GROWTH

4.1 Cohesive crack model

In the LEFM, the crack is traction free, but in the cohesive crack model, there is a non-zero traction on the crack surface.

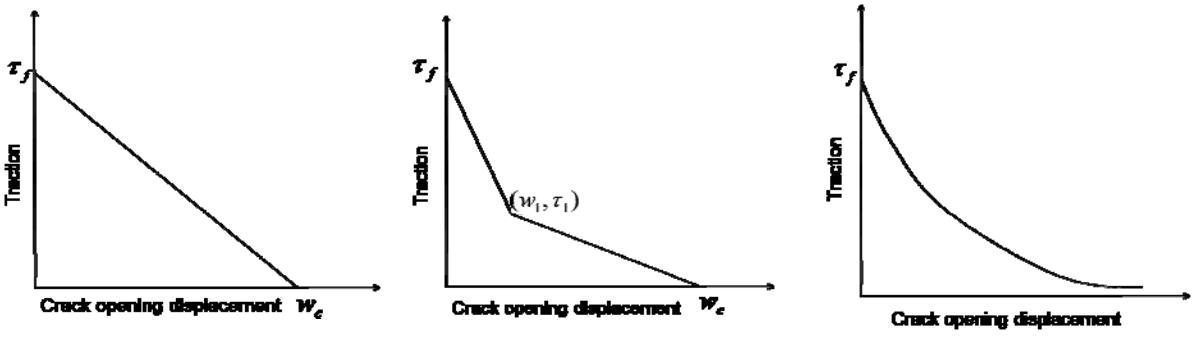

a. linear model b. bilinear model c. exponential reduction model

Figure 1. Various cohesive crack models

The traction stress is expressed by a function of crack opening displacement w or $[[\mathrm{u}]]$. Three different cohesive crack models widely used in practice are shown in Figure 1.

In this study, the linear and the bilinear models are used. For the case of the linear cohesive crack models, the traction stress is given by

$$\tau = \begin{cases} \tau_f \left(1 - \dfrac{w}{w_c}\right) & 0 \le w \le w_c \\ 0 & w > w_c \end{cases} \tag{25}$$

For the bilinear cohesive crack models, the traction stress is given by

$$\tau = \begin{cases} \dfrac{\tau_1 - \tau_f}{w_1} \cdot w + \tau_f & 0 \le w \le w_1 \\ \dfrac{\tau_1}{w_c - w_1}(w_c - w) & w_1 \le w \le w_c \\ 0 & w > w_c \end{cases} \tag{26}$$

The crack opening displacement is controlled by the enrichment terms of Equations (8) and (9), so

$$[[\mathrm{u}(\mathrm{X})]] = 2\sum_{n=1}^{n_C}\sum_{I\in W_b(\mathrm{X})} N_I(\mathrm{X})[[H_I(\mathrm{X})]]a_I^n + \sum_{m=1}^{m_t}\sum_{I\in W_S(\mathrm{X})} N_I(\mathrm{X})\sum_K [[B_K(\mathrm{X})]]\mathrm{b}_{IK}^m \quad (27)$$

In this study, the traction stress on the crack face is controlled by the normal component of the crack opening displacement. It means that the traction on the crack face is determined by $w = [[\mathrm{u}]]\cdot \mathrm{n}$

4.2 Analysis of static crack growth

Three different mixtures were used to prepare specimens for studying static and fatigue crack growth in the asphalt pavement. And the experiments were conducted under three different temperatures 10°C, 20°C and 30°C. For the dimensions of all the specimens, see Figure 2. The diameter is 150mm and the thickness is 50mm.

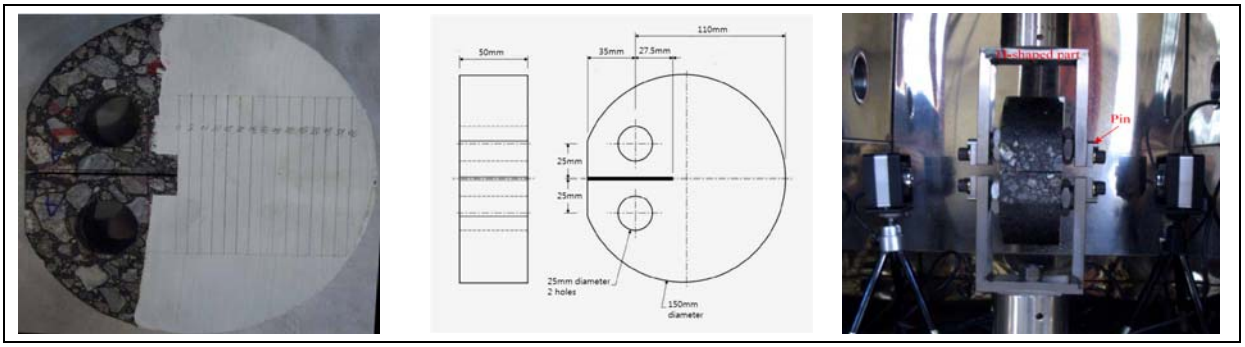

Figure 2. Test specimen and equipment

In the numerical experiment, the theory of XFEM is implemented by Matlab to simulate the experimental results. Figure 3 presents the numerical results. Three different crack lengths of, 10mm, 50mm and 80mm are illustrated. The results also represent distribution of cohesive traction on the crack face of the specimens. The graphs in Figure 3 show that within the fracture process zone the stress distribution reaches the peak value at crack tip and decreases behind the crack tip.

Crack length	10mm	50mm	80mm
Crack face	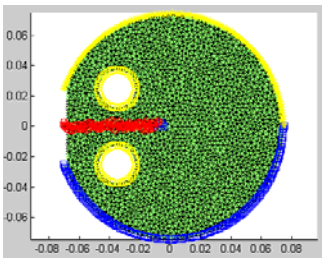	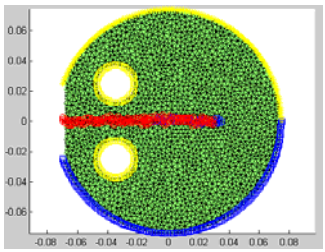	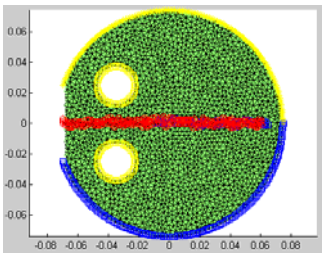
Stress distribution	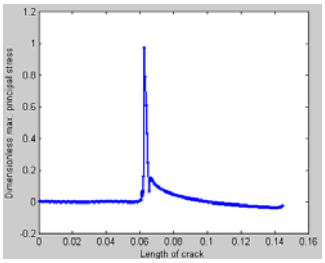	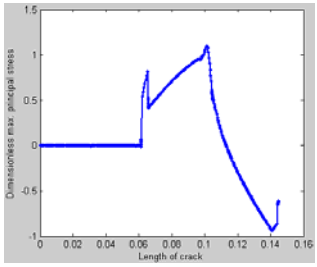	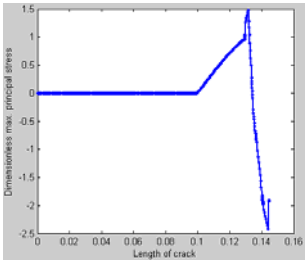
Deformed shape	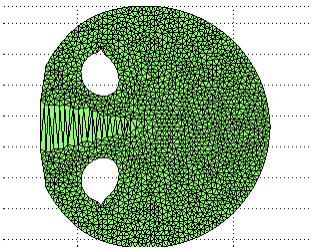	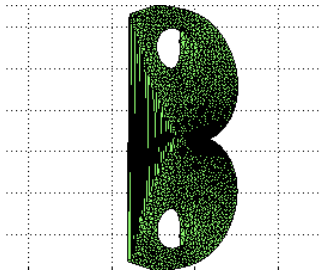	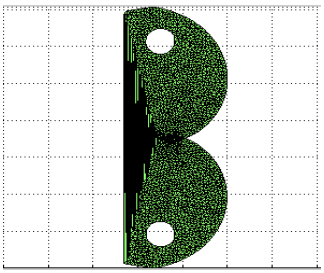

Figure 3. Crack growth, stress distribution, and shape of specimens

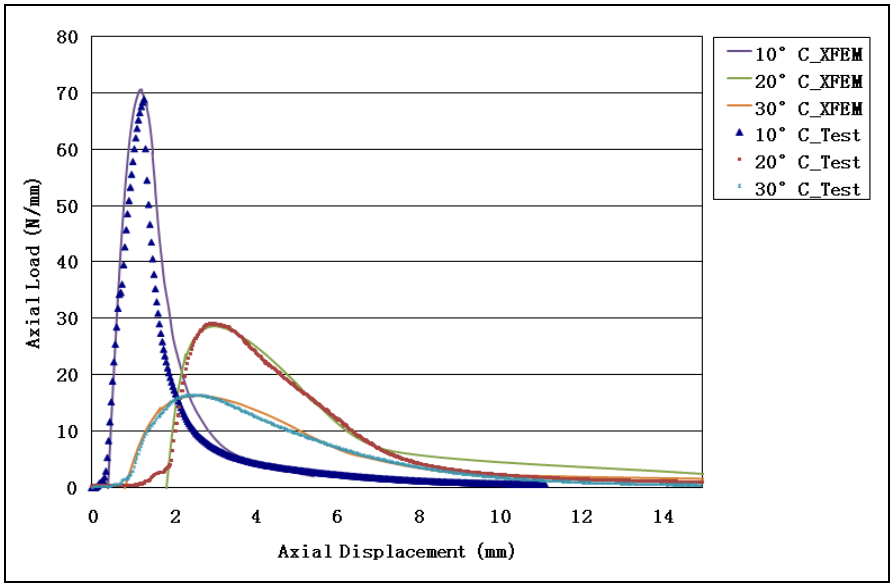

Figure 4. Load-displacement curve (with the linear cohesive crack model)

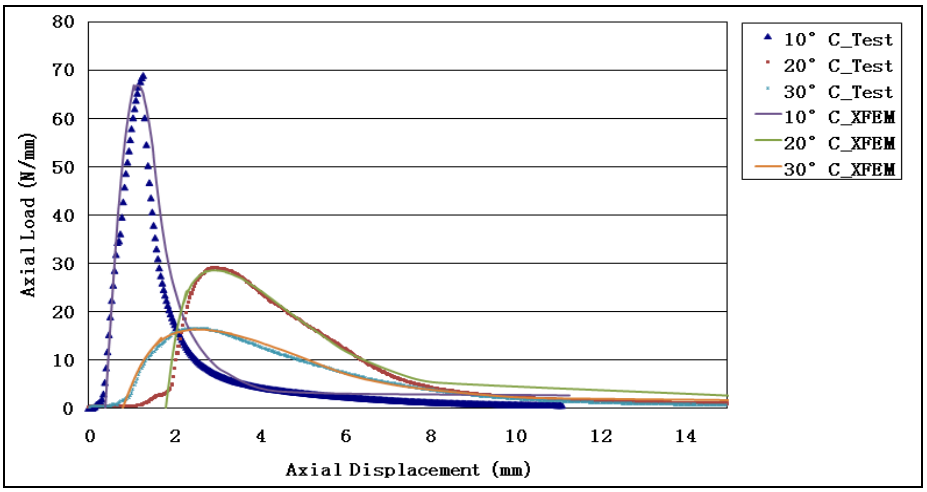

Figure 5. Load-displacement curve (with the bilinear cohesive crack model)

The test results and inverse estimation results by numerical experiments are shown in Figures 4 and 5. Symbols are the test results and solid lines are XFEM analysis results. Both of the linear cohesive model and the bilinear cohesive model can simulate the test results appropriately. And these Figures also show that as the temperature increases the Young's modulus and tensile strength of the asphalt falls rapidly. As the consequence of extensive inverse analysis with respect to the test results, the cohesive laws are identified as shown in Figure 6. The bilinear type of the cohesive law is also tried but the result is very close to that of the linear one as shown in Figure 6 (b).

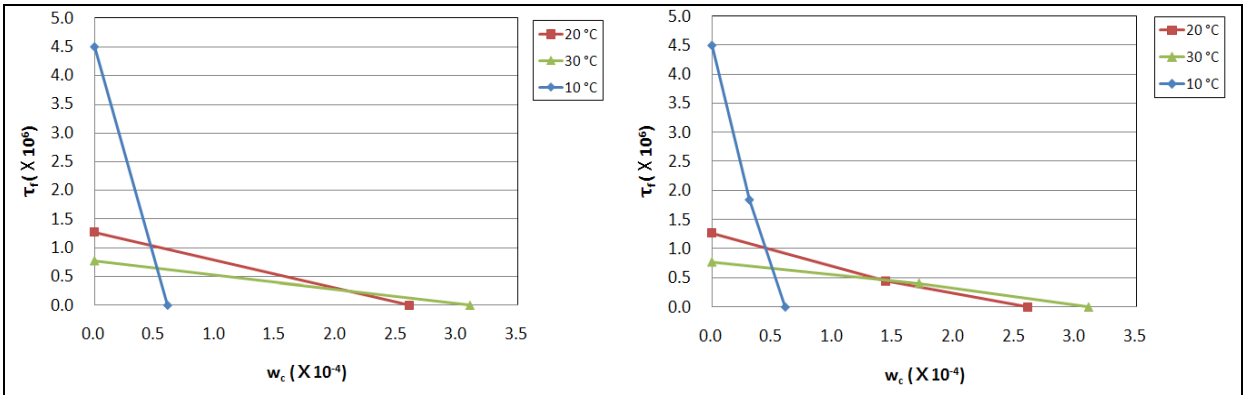

6-(a) linear model 6-(b) bilinear model

Figure 6. The cohesive crack models for different temperatures identified by a set of inverse analysis; (a) the linear model and (b) the bilinear model

The fracture energy which is the area under the cohesive law curve is given in Table 1.

Table 1. Fracture energy

Temperature	Fracture energy
10°C	270
20°C	330.2
30°C	238.7

Table 2. Inverse estimation of material properties (linear cohesive model)

Temp	Young's modulus [Pa]	Poisson ratio	τ_f [Pa]	w_c [m]
10°C	24×10^{9}	0.18	4.50×10^{6}	6.0×10^{-5}
20°C	12×10^{9}	0.18	1.27×10^{6}	2.6×10^{-4}
30°C	3.9×10^{9}	0.18	7.70×10^{5}	3.1×10^{-4}

Table 3. Inverse estimation of material properties (bilinear cohesive model)

Temp	Young's modulus [Pa]	Poisson ration	τ_f [Pa]	w_c [m]	τ_1 [Pa]	w_1 [m]
10°C	24×10^{9}	0.18	4.50×10^{6}	6.0×10^{-5}	1.845×10^{6}	3.06×10^{-5}
20°C	12×10^{9}	0.18	1.27×10^{6}	2.6×10^{-4}	4.445×10^{5}	1.43×10^{-4}
30°C	3.9×10^{9}	0.18	7.70×10^{5}	3.1×10^{-4}	4.081×10^{5}	1.075×10^{-4}

Table 2 and table 3 show the material properties and the cohesive crack parameters inversely estimated the linear and the bilinear ones. The initial slope of the load-displacement curve determines Young's modulus.

5. FATIGUE CRACK GROWTH

5.1 Paris' law

Paris' law is widely used because of its simplicity. The Paris' law is given by

$$\frac{da}{dN} = C(\Delta K)^m \tag{28}$$

Where a is crack length, N is number of load cycles, ΔK is the range of the stress intensity factor measured at the crack tip. *C* and *m* are material parameters.

5.2 Description of fatigue crack growth

The specimens for fatigue crack growth experiment are similar to those for static testing. Again, three different temperatures are considered for temperature effect on fatigue crack growth. The loads range change 200N, 250N and 300N, respectively with frequency 10Hz, 5Hz, 1Hz. Parameters of Paris' law, *C* and *m*, obtained by the inverse estimations are shown in table 4.

Table 4. Inverse estimation of parameters for Paris' law

Mixture type	Temperature	*C*	*m*
A type	10°C	5.00E-6	1.5725
	20°C	3.00E-6	1.6296
	30°C	5.40E-6	1.5976
B type	10°C	4.00E-6	1.5626
	20°C	9.00E-6	1.5648
	30°C	3.00E-6	1.6028

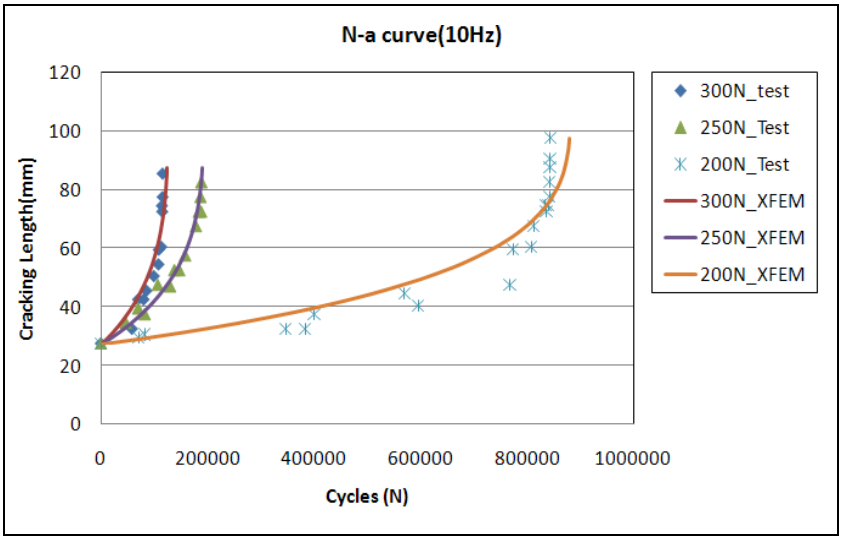

Figure 7. N-a curve for 200N, 250N, and 300N

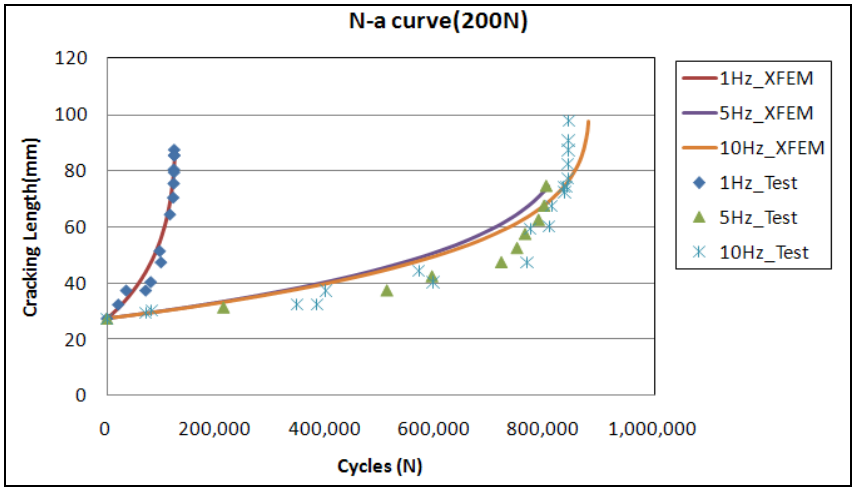

Figure 8. N-a curve for 1Hz, 5Hz, and 10Hz

The experimental data and the XFEM simulation are shown in Figures 7 and 8. The Figure 7 compares the results of three load ranges, 200N, 250N and 300N, at 10Hz frequency. In contract, the Figure 8 illustrates the results of the same cyclic load 200N at different frequencies, 1Hz, 5Hz and

10Hz. Those Figures show that simulation by XFEM combined with the Paris' law gives acceptable results.

6. CONCLUSIONS

The XFEM is applied to simulate static and fatigue crack growth. In static crack growth analysis, XFEM combines with the cohesive crack model and for fatigue crack growth analysis, XFEM is combined with the Paris' law. The analysis simulates the test results in a good agreement.

Although asphalt is a viscoelastic material, linear elastic constitutive equation was used for asphalt pavement in this study. For precisely considering loading velocity and temperature effects, viscoelasticity characteristics of asphalt is being considered later.

REFERENCE

1. Belytschko, T., Black, T. (1999). Elastic crack growth in finite elements with minimal remeshing. International Journal for Numerical Methods in Engineering, 45(5):601-620.

2. Belytschko, T; Chen, H; Xu, JX, et al (2003). Dynamic crack propagation based on loss of hyperbolicity and a new discontinuous enrichment. International journal for numerical methods in engineering. 58(12), 1873-1905.

3. Moes, N. Belytschko, T (2002). Extended finite element method for cohesive crack growth. Engineering fracture mechanics. 69(7) 813-833.

4. Moes, N. Dolbow, J. Belytschoko, T (1999). A finite element method for crack growth without remeshing. International journal for numerical methods in engineering. 46(1),131-150.

5. Paris, P.C. Erdogan, F (1963). A critical analysis of crack propagation laws. J. Basic Eng. 85, 528-534.

6. Ortiz, M. Pandolfi, A (1999). Finite-deformation irreversible cohesive elements for three-dimensional crack-propagation analysis. International journal for numerical methods in engineering. 44, 1267-1282.

7. Xu, XP. Needleman, A (1994). Numerical simulations of fast crack-growth in brittle solids. Journal of the mechanics and physics of solids. 42, 1397-&.

8. Zi, G., Belytschko, T. (2003). "New crack-tip elements for XFEM and applications to cohesive cracks." International Journal for Numerical Methods in Engineering 57(15), 2221-2240.

9. Zi, G., Chen, H., Xu, J., and Belytschko, T. (2005). "The extended finite element method for dynamic

fractures." Shock and Vibration 12(1), 9-23.

10. Zi, G. Song, J. Budyn, E. Lee, S. Belytschko, T (2004). A method for growing multiple cracks without remeshing and its application to fatigue crack growth. Institute of physics publishing. Modeling and simulation in materials science and engineering. 12, 901-915.